Korean J. Chem. Eng., **31**(9), 1641-1650 (2014)
DOI: 10.1007/s11814-014-0125-0

pISSN: 0256-1115
eISSN: 1975-7220

Improvement of thermal regeneration of spent granular activated carbon using air agent : Application of sintering and deoxygenation

Joon-Hyung Cho*, Yoon-Su Kim, Soo-Bin Jeon*, Jong-Beom Seo***, Jong-Hyeon Jung****, and Kwang-Joong Oh*,†**

*Department of Environmental Engineering, Pusan National University, San 30, Jangjeon-dong, Busan 609-735, Korea
**Division of Civil Construction & Business, Kolon Global Corporation, Byeolyangsangga2-ro, Gwacheon-si, Gyeonggy 427-709, Korea
***Technical Research Center, Ironmaking Technology Development Team, HyunDai Steel Company, Dangjin-si, Chungnam 343-711, Korea
****Faculty of Health Science, Daegu Haany University, Gyeongsan 712-715, Korea
(*Received 3 January 2014 • accepted 23 April 2014*)

Abstract–Thermal regeneration of spent granular activated carbon (GAC) using sintering, air-activation, and deoxygenation was investigated to determine the potential of this method for overcoming the drawbacks of thermal regeneration. The conditions for each step were optimized. The physicochemical properties of four regenerated GACs were assessed using BET, SEM, and FT-IR analysis. The suitability of the regenerated GACs for liquid-phase applications was assessed by phenol adsorption, using adsorption isotherms, kinetics, and thermodynamics. Sintering increased the micropore area and volume of regenerated GAC by 19% and 16%, respectively, and controlled excessive burn-off, reducing it by 19%. Air-activation has economic advantages because the reaction time is 80% less than that for steam-activation. Deoxygenation improved the maximum adsorption capacity by 7%, although the number of micropores was reduced. Regenerated GAC by sintering, air-activation, and deoxygenation was best for liquid-phase applications; the results show that these steps help to overcome the drawbacks of thermal regeneration.

Keywords: Thermal Regeneration, Sintering, Air-activation, Deoxygenation, Phenol Adsorption

INTRODUCTION

Granular activated carbon (GAC) is widely used in advanced drinking-water treatments to remove trace organic compounds, which have adverse effects on the environment and public health. However, once its adsorption capacity has been saturated, the spent GAC must be regenerated or replaced by a virgin adsorbent [1]. The former is preferable environmentally because otherwise the spent GAC would be incinerated or landfilled, and the latter has the disadvantages of high cost and the need for waste disposal [1,2]. GAC regeneration methods include bioregeneration, ultrasound, microwave, supercritical fluid, solvent, electrochemical, and thermal regeneration [1,3-5]. Thermal regeneration is the most widely used method in Europe, the US, and Korea [3,6]. However, it has a number of drawbacks: the micropores become wider because of thermal regeneration, reducing the ability to remove small molecular contaminants [4]; it is accompanied by excessive GAC burn-off [3,4]; it is energy intensive [3,4]; and there is a decrease in the adsorption capacity of GAC because of the formation of oxygen-containing groups on the carbon [7].

A number of studies aimed at overcoming these drawbacks of thermal regeneration have been reported. To overcome micropore extension and excessive burn-off, Mazyck and Cannon [8,9] investigated calcium sintering of spent GAC during the pyrolytic step using steam. The typical calcium content of field-spent GAC is 0.4-7.0 wt%, and the sintering effect using steam is similar to that under a N_2 or CO_2 atmosphere, but the sintering temperature is different with steam [9,10]. From the economic point of view, Sabio et al. [1] studied the thermal regeneration of spent GAC using air instead of steam and CO_2, which are generally used as activating agents. Air has advantages because it is free, and the processing time and heat requirements are low (heat requirement of air to reach the reaction temperature of 800 °C is one-fifth the enthalpy, expressed in kilograms per kilogram of agent, than that required with steam) [1, 11]. However, despite the economic advantages of using air as the activating agent, air-activation is seldom used because of the high reactivity of oxygen, which makes it difficult to control excessive carbon burn-off [1,12]. The surface oxygen groups on GAC are known to play an important role in the adsorption of organics, and its adsorption capacity decreases with increasing content of surface oxygen groups, which are formed on the carbon surface when steam, CO_2, or air is used in thermal regeneration [1,7,13,14]. To reduce the negative effect of the surface oxygen groups, Franz et al. [7] applied a deoxygenation process to GAC with surface oxygen groups under a constant flow of N_2 at 850 °C for 1 h.

In this study, to identify ways of overcoming these drawbacks, we investigated the effects of thermal regeneration of spent GAC with sintering, air-activation, and deoxygenation steps. A sintering step under an inert N_2 atmosphere was performed prior to the activation step to control micropore extension and excessive burn-off of GAC.

†To whom correspondence should be addressed.
E-mail: kjoh@pusan.ac.kr

Table 1. Iodine number and proximate analysis of spent granular activated carbon (GAC)

Sample	Iodine number (mg/g)	Moisture content (wt%)	Volatile matter (wt%)	Fixed carbon (wt%)	Ash (wt%)
Spent GAC	628.57	2.60	6.42	81.07	9.92

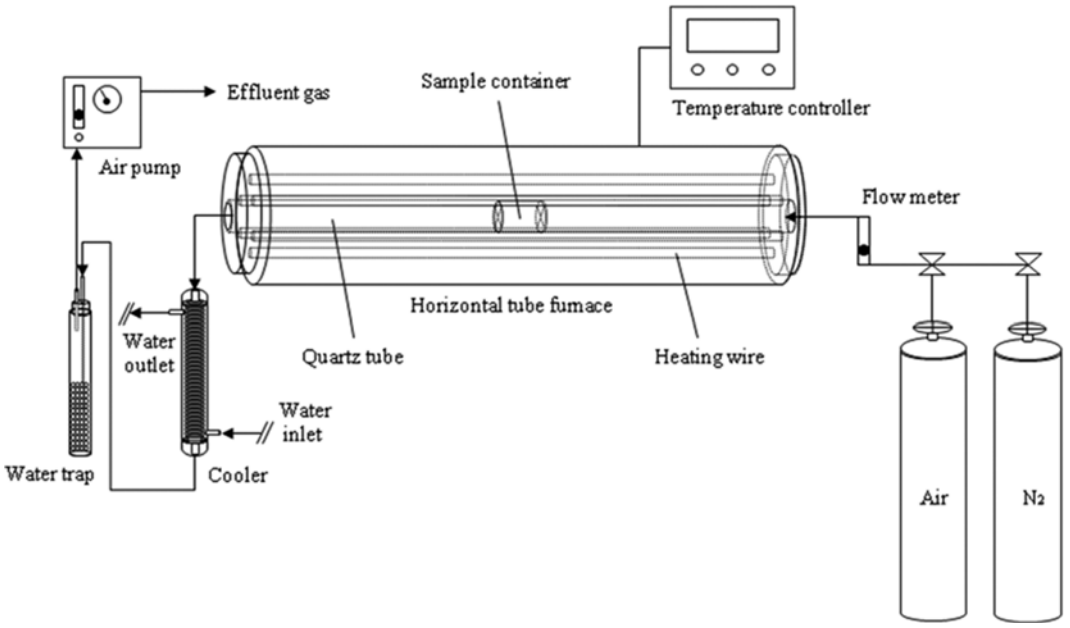

Fig. 1. Schematic diagram of thermal regeneration apparatus.

Activation using air was used to make the process more economic. The final deoxygenation step under an inert N_2 atmosphere was used to prevent a decrease in adsorption capacity because of the development of oxygen-containing groups on the GAC. As mentioned above, a number of studies on overcoming the drawbacks of thermal regeneration have been reported. However, to the best of our knowledge, there have been no previous reports of thermal regeneration using a series of sintering, air-activation, and deoxygenation steps. Thus, four thermal regeneration processes were tested: activation, sintering-activation, activation-deoxygenation, and sintering-activation-deoxygenation. First, the effects of different parameters were assessed to determine the optimum conditions for sintering, air-activation, and deoxygenation. Then, four thermally regenerated carbons were obtained using different combinations of these process with the optimum conditions, and the physicochemical properties of the regenerated carbons were assessed using nitrogen Brunauer-Emmett-Teller (BET) analysis, scanning electron microscopy (SEM), and Fourier-transform infrared (FT-IR) analysis. Finally, the suitability of the regenerated carbons for liquid-phase applications was assessed based on the adsorption of phenol, using adsorption isotherm, kinetic, and thermodynamic models.

MATERIAL AND METHODS

1. Spent GAC

The spent coal-based GAC used in this study was obtained from the Deok-san advanced water treatment facility in Daedong-myeon, Gimhae-si, Gyeongsangnam-do, Korea. The spent GAC was washed several times with deionized water to remove any foreign materials. The washed spent GAC was dried in a forced convection oven at 115±5 °C for 3 h. The dried GAC was sieved to a particle size of 0.595-2.380 mm. As shown in Table 1, the standard test methods in Korea (KS M 1802, 2009) [15] were used to determine the iodine number, and perform proximate analysis of the spent GAC.

2. Regeneration of Spent GAC

Thermal regeneration of the spent GAC was conducted using the laboratory-scale apparatus shown in Fig. 1. The apparatus consisted of a horizontal tube furnace, temperature controller, and gas-flow devices. The furnace was an STF-15/75/610 (Carbolite Ltd., Sheffield, UK), consisting of six heating wires, a sample container, and a quartz tube of external diameter 50 mm, thickness 3 mm, and length 1,000 mm. The temperature controller was a Eurotherm 2408CP with a programmable function, which controlled the temperature up to 1,500 °C, the heating rate, and the dwell time for each segment of the program. The gas-flow devices were divided into inflowing and outflowing parts. The former consisted of air (mixed N_2 79.00% and O_2 21.00%), a N_2 (99.99%) bombe, and a flow meter. The latter consisted of a cooler, water trap, and air pump. A Teflon tube also was used to connect the parts of the gas-flow devices.

To test the four thermal regeneration processes, regenerated samples were obtained using different combinations of the three individual steps: sintering, activation, and deoxygenation. The samples obtained were denoted by SA (sintering-activation), A (activation), AD (activation-deoxygenation), and SAD (sintering-activation-deoxygenation). In each experiment, the sample container with the dried spent GAC (4 g) was loaded into the furnace, and then the temperature was increased at a constant rate of 10 °C/min to different target temperatures for the individual steps under an inert low-oxygen atmo-

sphere as pyrolytic step. When the target temperature (500-800 °C) of the sintering step, during the pyrolytic step, was reached, the system was purged with a constant flow (1 L/min) of N_2 for sintering times of 0-60 min. When the target temperature (600-800 °C) of the activation step, after the pyrolytic step, was reached, the spent GAC was activated at flow rates of 0-3 L/min and activation times of 0-20 min. When the target temperature (800 °C) of the deoxygenation step, after activation step, was reached, a constant flow (1 L/min) of N_2 was allowed into the reactor for sintering times of 0-60 min. As soon as the thermal regeneration process was completed, the regenerated samples were taken out of the furnace, without cooling. Then the samples (AD, SAD) that included a deoxygenation step were cooled to room temperature under a flow of N_2 and stored in a N_2 atmosphere, and the other samples (A, SA) were cooled to room temperature in air.

The final products were characterized in terms of the BET surface area, pore structure distribution, burn-off, surface chemical structure, and surface microstructure. The BET surface area and pore structure distribution were obtained with a surface area and porosity analyzer (Micromeritics ASAP 2020, USA), using N_2 adsorption at −196 °C. The burn-off was calculated from the weight changes of the carbons after regeneration [16]. The surface chemical structure was examined using FT-IR spectroscopy (IRAffinity-1, Shimadzu, Japan). The surface microstructure was analyzed using field-emission SEM (FE-SEM; S-4200, Hitachi, Japan).

3. Phenol Adsorption

The stock solution for the tests was prepared by dissolving phenol (1.0 g, 99.5%; Sigma-Aldrich) in double-distilled water (1 L). Batch experiments on adsorption equilibrium were performed using a set of 250 mL round-bottomed flasks with stoppers; phenol solutions (200 mL) of different initial concentrations (50-200 mg/L) were added to each flask. Equal masses (0.20 g) of regenerated GACs, ground to powders (particle size <150 μm), were added to the phenol solutions, and each sample was kept in a shaking bath (SH-820F, Seyoung Scientific, KOR) at 125 rpm and 25±1 °C for 48 h to reach equilibrium. The solution pHs were not adjusted. A similar procedure was conducted using another set of round-bottomed flasks containing the same phenol concentrations without GAC, as blanks. The flasks were then removed from the shaker and the solutions were filtered with paper filters to minimize carbon fines interference with the analysis. The final concentration of the phenol solution was determined using ultraviolet-visible spectroscopy (UV mini 1240, Shimadzu, Japan) at 270 nm wavelength [17,18]. Prior to analysis, a calibration curve with at least five points was obtained, and it was very reproducible and linear over the concentration range used in this test. The amount of adsorbent at equilibrium, q_e (mg/g), was calculated as

$$q_e = \frac{(C_0 - C_e)V}{W} \quad (1)$$

where C_0 and C_e (mg/L) are the initial and equilibrium concentrations of phenol solution respectively, V (L) is the volume of the solution, and W (g) is the mass of dry adsorbent.

The procedure and liquid concentration analysis for the adsorption kinetics of phenol were the same as those used for equilibrium tests, except that samples were removed at time intervals between the initial and adsorption equilibrium time (0-48 h). In the adsorption thermodynamic experiments, the same method as that for the equilibrium tests was used, except that the tests were performed at different adsorption temperatures (10-40 °C).

The applicability of non-linear regression models was verified using two different error functions, i.e., the hybrid fractional error function (HYBRID), developed to improve the fit of the square-of-errors function at low concentration values, and Marquardt's percentage standard deviation (MPSD) error function, modified according to the number of degrees of freedom of a geometric mean error distribution [19].

RESULTS AND DISCUSSION

1. Thermal Regeneration Process Optimization

1-1. Sintering

The purpose of sintering in the thermal regeneration process is to cause a surface loss of catalytic calcium species loaded in the porous structure of the spent GAC, at sufficiently high temperature [8,9]; these species are $Ca(OH)_2$, $CaCO_3$, $CaSO_4$, CaO, and metal-organic complexes, which are present in natural water, precipitation chemicals in water treatment processes [20,21]. Sintering is strongly dependent on temperature such as the semi-empirical Tammann temperature, defined as 0.5 times the melting point of the catalytic material [22]. When this temperature is reached, the migration of catalytic surface atoms increases and the catalytic surface area decreases because of crystallite growth [22,23]. The Tammann temperatures for $Ca(OH)_2$, $CaCO_3$, $CaSO_4$, and CaO, based on the melting points, are about 290, 533, 730, and 1,307 °C, respectively [24].

Fig. 2 shows the burn-off of GAC samples with respect to sintering temperature and time, at a N_2 flow rate of 1 L/min, as a result of using an air-activation step at 800 °C for 3 min (denoted as zero sintering time) after the sintering tests. As shown, for the first 15 min, the burn-off rates decline sharply and then the rates gradually increase. The optimum conditions for the minimum burn-off are a sintering temperature of 600 °C, sintering time of 15 min, with a

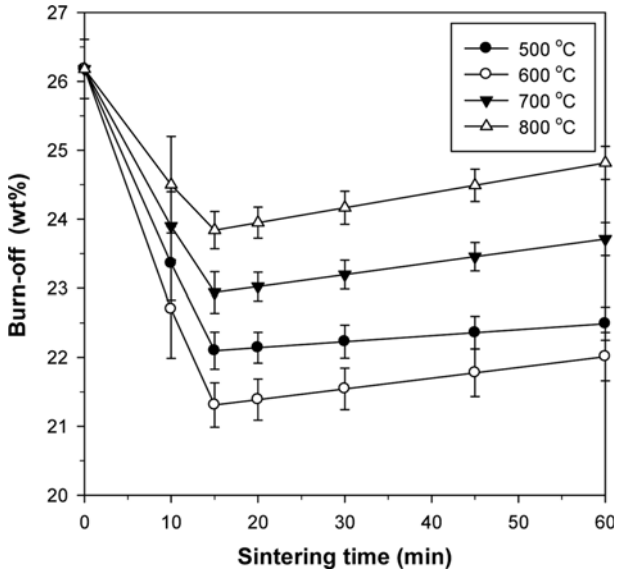

Fig. 2. Burn-off of granular activated carbon samples with respect to sintering temperature and time (N_2 flow rate: 1.0 L/min).

burn-off of 21.31 wt%. These results are associated with the reduction of catalyst active surface due to crystallite growth of the calcium species for the initial 0-15 min [22,23], and then the slight burn-off of carbon base occurs by thermal stress. When the sintering temperature reaches 600 °C, above the Tammann temperature for $CaCO_3$, the prevalent form of calcium on spent GAC [25], the main surface loss of calcium occurs, and ramping the activation temperature to 800 °C, above the Tammann temperature for $CaSO_4$, also reduces the catalytic properties. Although CaO is a thermodynamically stable species, CaO sintering at temperatures greater than 700 °C in N_2 is well known [8]. Generally, a high sintering temperature is desirable for the reduction of surface catalytic calcium species loaded in the porous structure of spent GAC; however, this causes excessive burn-off and damages the physical properties of the GAC because of thermal stress.

1-2. Air-activation

When air as the oxidizing agent reacts with carbon, an exothermic reaction occurs, unlike the case for steam or CO_2. The reaction is difficult to control and excessive carbon burn-off easily occurs, resulting in destruction of the original carbon pore structure [12]. It is therefore important to identify the optimum conditions for the activation step; these depend on parameters such as the activation temperature and time, and the air flow rate.

Fig. 3 shows the iodine numbers of GAC samples with respect to activation temperature and time at an air flow rate of 1 L/min, and with respect to air flow rate at an activation temperature of 800 °C and an activation time of 3 min; activation was performed after pyrolytic steps as different activation temperatures. The iodine number is an indicator of carbon porosity, measured as the number of milligrams of iodine adsorbed per gram of activated carbon in solution [26]. As can be seen from Fig. 3(a), the maximum iodine number increases with increasing activation temperature. In Fig. 3(b), the iodine number increases for the initial 0-1 L/min, and subsequently, the value decreases as the air flow rate increases. The conditions to obtain the maximum iodine number are therefore an activation temperature of 800 °C, activation time of 3 min, and air flow rate of 1 L/min, giving an iodine number of 932.93 mg/g. These results indicate that operating beyond the optimum conditions during the activation step has a negative effect on the carbon porous structure. Although a detailed comparison is not available because of the different characteristics of the spent GACs, air-activation could have economic advantages, because the reaction time is 80% less than for steam-activation (reaction time is 15 min at activation temperature of 800 °C, steam flow rate of 4.0 L/min) [2].

1-3. Deoxygenation

To decrease the number of surface oxygen groups and increase the adsorption capacity of the carbon for liquid organics, deoxygenation is applied. However, because thermal treatment of the carbon for a long time at high temperature induces collapse of the porous structure, it is necessary to examine the carbon porosity in the deoxygenation step.

Fig. 4 shows the iodine numbers of GAC samples with respect

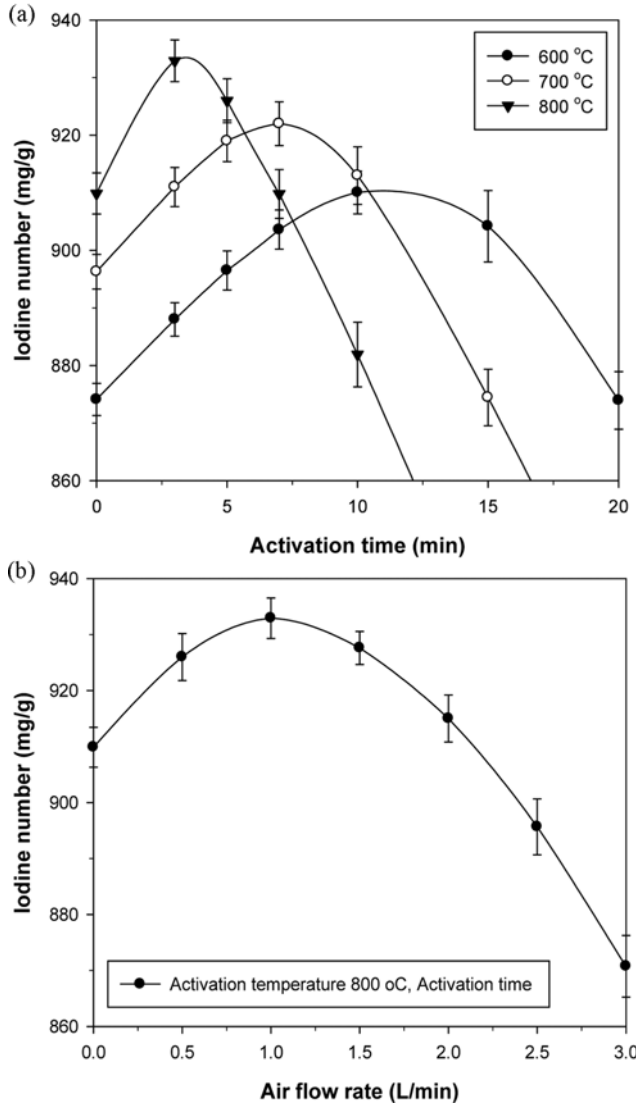

Fig. 3. Iodine numbers of granular activated carbon samples with respect to activation temperature and time (air flow rate: 1 L/min), and air flow rate (activation temperature: 800 °C, activation time: 3 min).

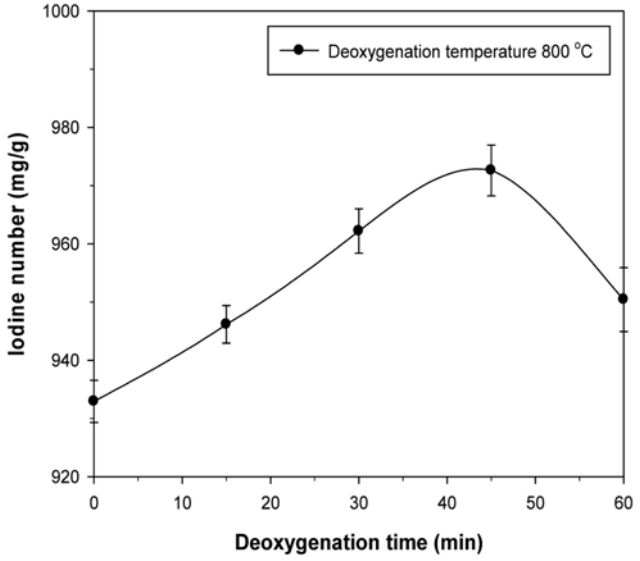

Fig. 4. Iodine numbers of granular activated carbon samples with respect to deoxygenation time (deoxygenation temperature: 800 °C).

to deoxygenation time at 800 °C; deoxygenation was performed after activation at 800 °C for 3 min. The figure shows that for the first 45 min, the iodine number gradually increases, but then it sharply decreases. This is associated with the destruction of the porous structure after deoxygenation for 45 min. Franz et al. [7] reported that the pore structure of a carbon sample might collapse because of high-temperature deoxygenation. The optimum condition for minimizing the number of oxygen-containing groups, without negatively affecting the pore structure, is a deoxygenation time of 45 min at 800 °C.

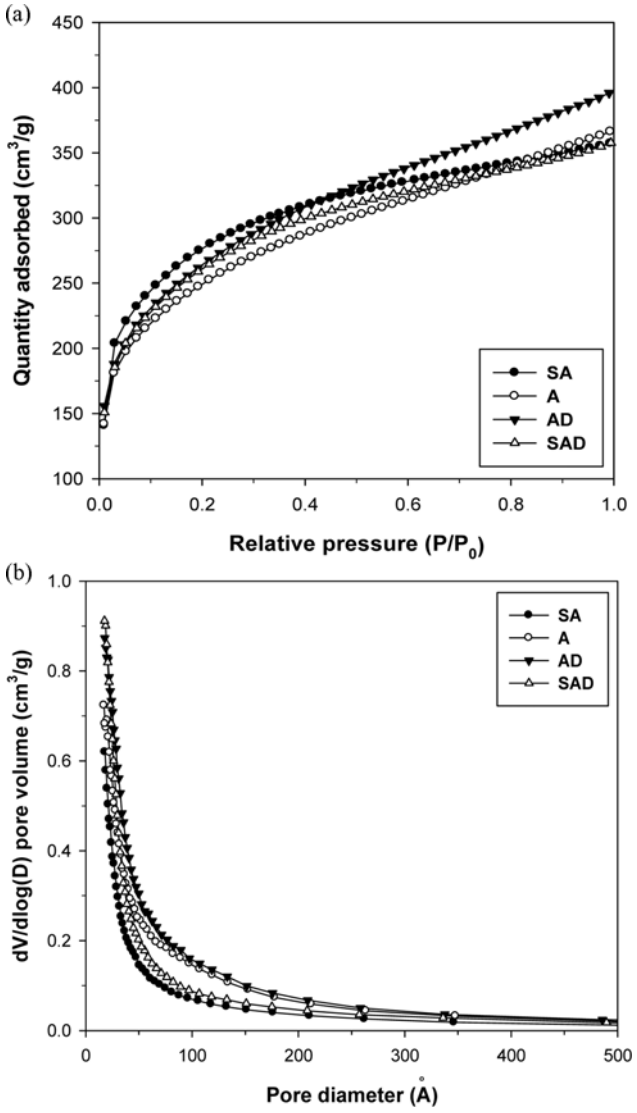

Fig. 5. N_2 adsorption isotherms and pore size distributions of thermally regenerated granular activated carbons.

2. Physicochemical Properties of Thermally Regenerated GACs

2-1. Surface Area and Pore Structure Distribution

Four thermally regenerated carbons (SA, A, AD, and SAD) were obtained by using different combinations of steps under the optimum conditions. The N_2 adsorption isotherms and pore size distributions for the samples are shown in Fig. 5. The quantities adsorbed on the four thermally regenerated GACs increase sharply at low relative pressures, indicating filling of the micropores with N_2, and the quantities increase gradually with increasing relative pressure up to P/P_0=1 (Fig. 5(a)). The different adsorption isotherm shapes by the samples are related to pore size distributions. SA and SAD have a concave shape of low slope in 0.4-1.0 P/P_0 due to multilayer adsorption on small external pores. Samples A and AD, without sintering steps, have a linearly increasing middle-late section of relatively high slope due to large external pores. These results indicate that the sintering step has a positive effect on decreasing the reactivity between carbon and air during the activation step, resulting in loss of surface catalytic calcium surface. Savova et al. [27] found that oxidation with air of a carbonized material produces a predominantly macroporous structure because the oxygen reacts at the pore entrances and does not penetrate into the narrow pores because of its high reactivity. The pore size distributions in Fig. 5(b) show that if there is no sintering, extensive oxidation occurs in the mesoporous structure before the air penetrates into the micropores.

Table 2 lists the surface areas, pore volumes, and average pore diameters of virgin, spent, and thermally regenerated GACs. A comparison of the total surface areas, micropore areas, and volumes of the regenerated samples shows that sintering leads to increases of about 8%, 19%, and 16%, respectively, for SA compared with A. The average pore diameter for the regenerated GACs also shows that if there is no sintering, the value is greater because of the catalytic effect of calcium species. In contrast, the micropore area and volume of AD, with deoxygenation, are about 9% and 7%, respectively, less than those for A. This slight reduction is attributed to the collapse of micropores because of thermal stress in the high-temperature treatment. The surface areas of A and SAD are close to each other because of sintering and deoxygenation interactions.

In this work, lower recovery rates, between 72-78% of the surface areas of virgin GACs, were obtained (recovery is usually 60-95% of the levels in virgin GAC for steam regeneration) [2]. The recovery rates depend on the characteristics of the spent GAC. The mesopore volume of spent GAC is higher than that of virgin GAC,

Table 2. Surface areas, pore volumes, and average pore diameters of virgin, spent, and thermally regenerated granular activated carbons

Sample	Total surface area (m^2/g)	Micropore area (m^2/g)	Mesopore volume (cm^3/g)	Micropore volume (cm^3/g)	Average pore diameter (Å)
Virgin GAC	1285	1177	0.105	0.487	18.43
Spent GAC	749	524	0.189	0.255	22.25
SA	1001	741	0.212	0.341	22.08
A	931	624	0.255	0.294	25.31
AD	948	565	0.338	0.274	25.85
SAD	937	632	0.254	0.299	23.60

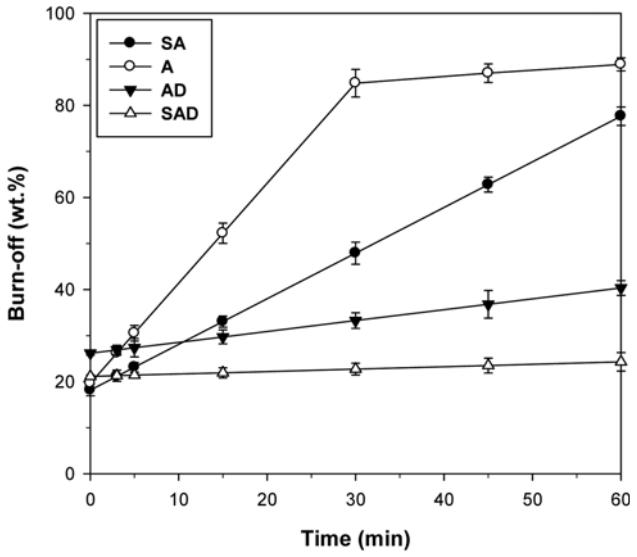

Fig. 6. Burn-offs of thermally regenerated granular activated carbons with respect to processing time.

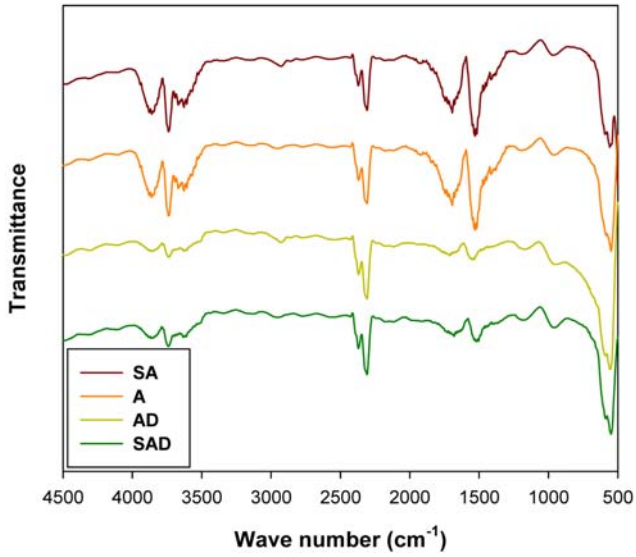

Fig. 7. Fourier-transform infrared spectra of thermally regenerated granular activated carbons.

as shown in Table 2. This indicates that some of the mesopores in the original carbon structure were destroyed by the previous thermal regeneration cycles in the water treatment facility.

2-2. Burn-off

The extent of the carbon burn-off is the key parameter in a thermal regeneration process as it determines the amount of final product [2,28]. Fig. 6 shows the burn-offs of thermally regenerated GACs with respect to processing time, obtained by measuring the weight changes of the carbons in each final step during thermal regeneration at 800 °C. The burn-offs for SA, A, AD, and SAD under the optimum conditions were 21.3, 26.2, 36.8, and 23.5 wt%, respectively. Compared with the burn-off in the general steam regeneration process (total burn-off is 17-32 wt%, consisting of 12-22 and 5-10 wt% in the pyrolytic and activation steps, respectively) [2], the burn-off for A, consisting only of an air-activation step, was higher; however SA and SAD, which included sintering steps, had lower values. The burn-off rates for SA, A, AD, and SAD were 39.7, 86.9, 9.4, and 2.1 mg/min, respectively. Compared with the carbon burn-off rate during the steam-activation step (burn-off rate is 48.7-76.2 mg/min at 800 °C) [2], the burn-off rate for A was greater, but the value for SA was lower, than the minimum value of 48.7 mg/min in steam regeneration. These results show that the additional sintering step can control excessive carbon burn-off during air-activation. As can also be seen from the burn-off rates for AD and SAD, this sintering effect plays a role during the deoxygenation step, and it is considered that the oxygenated sites formed on the GAC surface during air-activation influence the catalytic reaction in the deoxygenation step.

2-3. Surface Chemical Structure

It has been reported that an increase in the number of surface oxygen groups on the carbon decreases the adsorption capacity for liquid organics by a water adsorption mechanism, in which water clusters form on the surface oxygen groups, hindering migration of organics into smaller pores [7,14]. It is therefore important to analyze the GAC surface chemical structure.

Fig. 7 shows the FT-IR spectra of the four thermally regenerated GACs. The absorbance bands are interpreted by information from prior studies [29-33]. In the SA and A samples, which had a final air-activation step, peaks representing hydroxyl, carboxyl, and carbonyl groups were observed at 3,800-3,700 (stretching vibration of O-H in kaolinite), 1,700 (stretching vibration of C=O in carboxyl acid group), and 1,560 cm^{-1} (stretching vibration of C=O in diketone, keto-ester and keto-enol), respectively [31-33]. Sabio et al. [1] reported that oxygen-containing groups such as hydroxyl, carboxylic, and carbonyl groups are formed on carbon during thermal regeneration using air. These results are in agreement with the spectra of the SA and A samples. For the AD and SAD samples, with a final deoxygenation step, the intensities of all these peaks (hydroxyl, carboxyl, and carbonyl groups) were reduced. In other peaks, there are no significant changes. These results show that the deoxygenation step effectively reduces the number of surface oxygen groups formed during activation.

2-4. Surface Microstructure

The surface microstructures of the spent and thermally regenerated GACs were examined using FE-SEM at a magnification of 20,000×; the images are shown in Fig. 8. As can be seen in Fig. 8(a), there are impurities on the surface of the spent GAC. The impurities are removed from the surface after regeneration, as can be seen in Fig. 8(b)-(e).

3. Phenol Adsorption

3-1. Adsorption Isotherms

It is necessary to carry out adsorption experiments to assess the suitability of regenerated GACs for contaminant removal from solutions, because the physicochemical properties of GACs influence their adsorption capacities [1]. Adsorption isotherms provide information useful for optimizing the design of adsorption systems for removing adsorbates [19].

The adsorption experimental data were plotted, based on adsorption isotherms, using two-parameter models, i.e., the Langmuir, Freundlich, and Temkin models, and three-parameter models, i.e., the Redlich-Peterson and Toth models, using non-linear methods [19], as shown in Fig. 9. The estimated parameters for the adsorption isotherm mod-

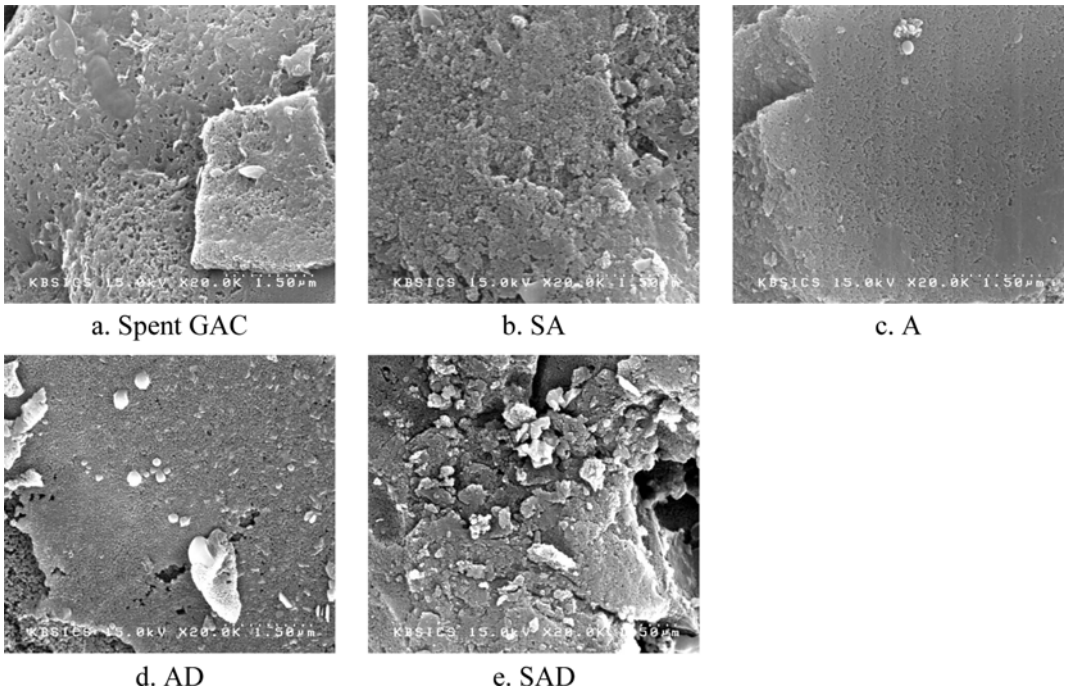

Fig. 8. Field-emission scanning electron microscopy images of spent and thermally regenerated granular activated carbons (magnification 20,000×).

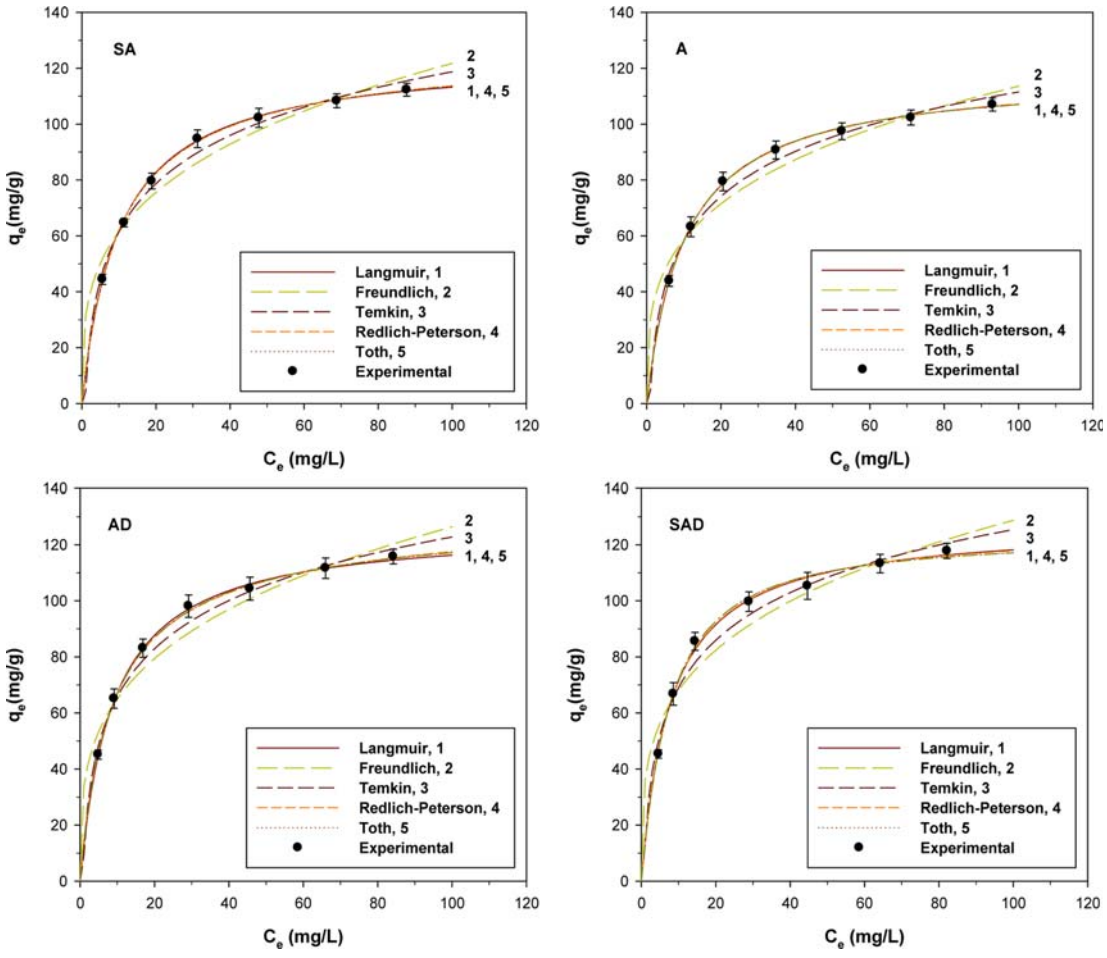

Fig. 9. Equilibrium isotherms for removal of phenol by thermally regenerated granular activated carbons at 25 °C.

Table 3. Isotherm parameters for removal of phenol by thermally regenerated granular activated carbons at 25 °C

Adsorbent	q_m (mg/g)	K_L (L/mg)	R^2	HYBRID	MPSD
Langmuir					
SA	124.747	0.098	0.999	0.118	0.167
A	118.001	0.098	0.999	−0.134	0.189
AD	126.581	0.113	0.999	0.264	0.373
SAD	127.444	0.127	0.997	−1.012	1.431
Adsorbent	K_F [(mg/g)/(mg/L)$^{1/n}$]	1/n	R^2	HYBRID	MPSD
Freundlich					
SA	31.084	3.373	0.983	−4.008	5.668
A	30.246	3.481	0.983	−3.735	5.282
AD	33.374	3.459	0.984	−4.026	5.693
SAD	35.910	3.608	0.977	−5.018	7.097
Adsorbent	K_T (L/mg)	B_1	R^2	HYBRID	MPSD
Temkin					
SA	1.185	24.865	0.996	−1.005	1.422
A	1.220	23.210	0.995	−1.088	1.538
AD	1.420	24.770	0.996	−1.019	1.441
SAD	1.662	24.518	0.991	−1.864	2.635
Adsorbent	K_R (L/g)	a_R (L/mg)	β	R^2	HYBRID	MPSD
Redlich-Peterson						
SA	12.733	0.109	0.985	0.999	−0.157	0.220
A	11.710	0.103	0.993	0.999	−0.451	0.631
AD	15.575	0.144	0.966	0.999	−0.413	0.578
SAD	15.902	0.120	1.009	0.997	−1.822	2.551
Adsorbent	q_e^{∞} (mg/g)	K_{Th} [(mg/L)Th]	Th	R^2	HYBRID	MPSD
Toth						
SA	126.562	8.825	0.954	0.999	−0.120	0.168
A	118.021	10.234	0.999	0.999	−0.275	0.385
AD	131.021	6.480	0.894	0.999	−0.315	0.442
SAD	123.513	11.598	1.135	0.997	−1.082	1.514

els are presented in Table 3. A comparison of the correlation and error function values for the regenerated GACs shows that the adsorption equilibrium data best match the Langmuir isotherm model. According to the results for the Langmuir isotherm, the maximum adsorption capacities of SA, AD, and SAD are about 6%, 7% and 8%, respectively, more than that of A.

To identify the effects of the chemical structures on the adsorption capacities of the regenerated GACs, the maximum adsorption capacity was normalized for differences among the total surface areas to minimize the influence of the surface area. The normalized adsorption capacities of AD and SAD are 6% and 7%, respectively, more than that of A. The values for SA and A are close to each other, with the SA value being 2% less than that for A. These results show that deoxygenation leads to an increase in the chemical adsorption capacity for the liquid phase by reducing the number of surface oxygen groups.

3-2. Adsorption Kinetics

The adsorption kinetic data are useful in predicting the equilibrium capacity of an adsorbent from the initial adsorption data before the equilibrium state is reached. The experimental adsorption data at an initial phenol concentration of 50 mg/L were used to determine whether the adsorption kinetics fitted a pseudo-first-order or pseudo-second-order model [34]. The kinetic parameters, and correlation and error function values are listed in Table 4. A comparison of the correlation and error function values for the regenerated GACs shows that the adsorption kinetic data match the pseudo-second-order model better. The experimental equilibrium capacities of the regenerated GACs for the second-order model are predicted well by the calculated values. These results show that the pseudo-second-order kinetic model provides a better correlation for the adsorption of phenol onto the regenerated GACs than the pseudo-first-order model does.

3-3. Thermodynamics

Thermodynamic data provide entropy and energy factors for determining the degree of spontaneity of an adsorption process. A Gibbs free-energy change (ΔG^{o}) with a higher negative value indicates a more energetically favorable adsorption [35]. The equilibrium constants obtained from the best-fitted Langmuir isotherm model were used to determine the Gibbs free-energy changes at 10, 25, and 40 °C, as described in the literature [35,36]. Fig. 10 shows the van't Hoff

Table 4. Kinetic parameters for removal of phenol by thermally regenerated granular activated carbons at 25 °C

Adsorbent	k_1 (min^{-1})	$q_{e,exp}$ (mg/g)	$q_{e,cal}$ (mg/g)	R^2	HYBRID	MPSD
Pseudo-first-order						
SA	0.174	44.416	22.861	0.997	16.177	28.019
A	0.156	43.872	26.212	0.998	13.418	23.240
AD	0.141	45.146	23.089	0.992	16.286	28.208
SAD	0.179	45.392	24.524	0.998	15.324	26.542
Adsorbent	k_2 [g/(mg/min)]	$q_{e,exp}$ (mg/g)	$q_{e,cal}$ (mg/g)	R^2	HYBRID	MPSD
Pseudo-second-order						
SA	0.020	44.416	44.248	0.995	0.126	0.218
A	0.015	43.872	43.668	0.994	0.155	0.268
AD	0.020	45.146	43.478	0.995	1.232	2.133
SAD	0.018	45.392	45.872	0.997	−0.352	0.611

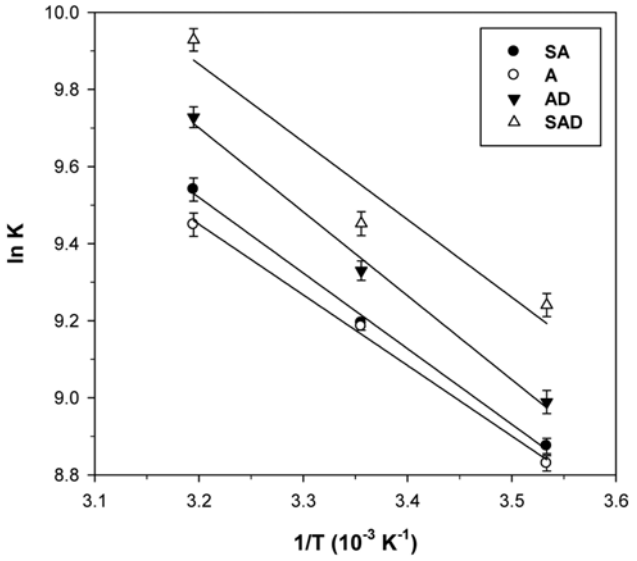

Fig. 10. van't Hoff plots of adsorption equilibrium constants, K, using Langmuir isotherms.

Table 5. Thermodynamic parameters for phenol removal by thermally regenerated granular activated carbons at different temperatures

Temperature (°C)	K_L (L/mg)	$-\Delta G^o$ (kJ/mol)	ΔH^o (kJ/mol)	ΔS^o [kJ/(mol K)]
SA				
10	0.072	−20.882	-	-
25	0.098	−22.780	-	-
40	0.139	−24.827	-	-
			16.310	0.132
A				
10	0.068	−20.776	-	-
25	0.098	−22.757	-	-
40	0.127	−24.589	-	-
			15.224	0.128
AD				
10	0.080	−21.150	-	-
25	0.113	−23.115	-	-
40	0.168	−25.315	-	-
			18.096	0.139
SAD				
10	0.103	−21.742	-	-
25	0.127	−23.418	-	-
40	0.205	−25.837	-	-
			16.767	0.136

plots for the Langmuir isotherms, from which the thermodynamic parameters were obtained. Table 5 shows the thermodynamic parameters for phenol removal by the thermally regenerated GACs at different temperatures. A comparison of the negative ΔG^o values shows that the value increases with an increase in adsorption temperature, because phenol adsorption is endothermic. The value for SAD at each adsorption temperature is the highest among the regenerated GACs. These results show that sintering, air-activation, and deoxygenation steps produce regenerated GACs that give the most thermodynamically favorable adsorption for the removal of liquid phenol.

CONCLUSIONS

Experimental results show that sintering prevented widening of the micropores; the micropore area and volume were about 19% and 16%, respectively, more than those without sintering, and excessive burn-off caused by air-activation was reduced by as much as 19%. Air-activation could have economic advantages, because the reaction time is 80% less than that for steam-activation. Deoxygenation improved the chemical adsorption properties for liquid phases, with the maximum adsorption capacity being 7% more than in the case of no deoxygenation. The thermally regenerated GAC produced by a series of sintering, air-activation, and deoxygenation steps was the most suitable for liquid-phase applications. These results show that a series of sintering, air-activation, and deoxygenation steps can contribute to overcoming the drawbacks of thermal regeneration.

This study showed that although a thermal regeneration process with sintering, air-activation, and deoxygenation steps still has limitations, such as a lower recovery rate and higher burn-off because of the characteristics of the spent GAC and the inert conditions in

the pyrolytic step, respectively, it has the potential to overcome the drawbacks of the previous thermal regeneration processes. Air is seldom used as the activating agent in thermal regeneration processes because of its high reactivity, which can cause excessive GAC burn-off. However, we were able to control the burn-off. Air has economic advantages because it is free, and the processing time and heat requirements are low.

ACKNOWLEDGEMENT

This work was supported by the Brain Korea 21 Plus Project in the Division of Creative Low Impact Development and Management for Ocean Port City Infrastructures.

REFERENCES

1. E. Sabio, E. González, J. F. González, C. M. González-García, A. Ramiro and J. Gañan, *Carbon*, **42**, 2285 (2004).
2. G. San Miguel, S. D. Lambert and N. J. D. Graham, *Water Res.*, **35**, 2740 (2001).
3. A. L. Cazetta, O. P. Junior, A. M. M. Vargas, A. P. da Silva, X. Zou, T. Asefa and V. C. Almeida, *J. Anal. Appl. Pyrol.*, **101**, 53 (2013).
4. R. M. Narbaitz and J. McEwen, *Water Res.*, **46**, 4852 (2012).
5. B. Lai, Y. X. Zhou and P. Yang, *J. Chem. Technol. Biotechnol*., **88**, 474 (2013).
6. S. Román, B. Ledesma, A. Álvarez-Murillo and J. F. González, *Fuel Process. Technol.*, **116**, 358 (2013).
7. M. Franz, H. A. Arafat and N. G. Pinto, *Carbon*, **38**, 1807 (2000).
8. D. W. Mazyck and F. S. Cannon, *Carbon*, **38**, 1785 (2000).
9. D. W. Mazyck and F. S. Cannon, *Carbon*, **40**, 241 (2002).
10. F. S. Cannon, *Carbon*, **32**, 1285 (1994).
11. H. McLaughlin, *Int. Sugar J.*, **107**, 112 (2005).
12. K. S. Ryoo, T. D. Kim and Y. H. Kim, *Bull. Korean Chem. Soc.*, **23**, 817 (2002).
13. S. Román, B. Ledesma, A. Álvarez-Murillo and J. F. González, *Fuel Process. Technol.*, **116** 358 (2013).
14. P. Pendleton, S. H. Wu and A. Badalyan, *J. Colloid Interface Sci.*, **246**, 235 (2002).
15. KSM 1802, *Test methods for activated carbon*, Korea Industrial Standards, Korean Agency for Technology and Standards (2009).
16. Z. Zhang, W. Qu, J. Peng, L. Zhang, X. Ma, Z. Zhang and W. Li, *Desalination*, **249**, 247 (2009).
17. B. H. Hameed and A. A. Rahman, *J. Hazard. Mater.*, **160**, 576 (2008).
18. A. T. M. Din, B. H. Hameed and A. L. Ahmad, *J. Hazard. Mater.*, **161**, 1522 (2009).
19. V. C. Srivastava, M. M. Swamy, I. D. Mall, B. Prasad and I. M. Mishra, *Colloids Surf., A.*, **272**, 89 (2006).
20. N. D. McCafferty, M. E. Callow, L. Hoggett, B. Holden and B. S. C. Leadbeater, *Water Res.*, **34**, 2199 (2000).
21. D. Clifford, S. Subramonian and T. J. Sorg, *Environ. Sci. Technol.*, **20**, 1072 (1986).
22. J. A. Moulijn, A. E. V. Diepen and F. Kapteijn, *Appl. Catal. A- Gen.*, **212**, 3 (2001).
23. C. H. Bartholomew, *Appl. Catal. A-Gen.*, **212**, 17 (2001).
24. J. H. Yang, S. M. Shih and P. H. Lin, *Ind. Eng. Chem. Res.*, **51**, 2553 (2012).
25. G. San Miguel, S. D. Lambert and N. J. D. Graham, *Appl. Catal. B-Environ.*, **40**, 185 (2003).
26. R. Yan, D. T. Liang, L. Tsen, Y. P. Wong and Y. K. Lee, *Fuel*, **83**, 2401 (2004).
27. D. Savova, E. Apak, E. Ekinci, F. Yardim, N. Petrov, T. Budinova, M. Razvigorova and V. Minkova, *Biomass Bioenergy*, **21**, 133 (2001).
28. D. Xin-hui, C. Srinivasakannan, W. W. Qu, W. Xin, P. Jin-hui and Z. Li-bo, *Chem. Eng. Process.*, **53**, 53 (2012).
29. B. Lai, Y. Zhang, Z. Chen, P. Yang, Y. Zhou and J. Wang, *Appl. Catalysis. B-Environ.*, **144**, 816 (2014).
30. B. Lai, Y. Zhou and P. Yang, *Chem. Eng. J.*, **200-202**, 10 (2012).
31. C. H. Cheng, J. Lehmann, J. E. Thies, S. D. Burton and M. H. Engelhard, *Org. Geochem.*, **37**, 1477 (2006).
32. I. H. Yoon, X. Meng, C. Wang, K. W. Kim, S. Bang, E. Choe and L. Lippincott, *J. Hazard. Mater.*, **164**, 87 (2009).
33. A. Swiatkowski, M. Pakula, S. Biniak and M. Walczyk, *Carbon*, **42**, 3057 (2004).
34. S. Azizian, *J. Colloid Interface Sci.*, **276**, 47 (2004).
35. A. Y. Dursun and Ç. S. Kalayci, *J. Hazard. Mater.*, **123**, 151 (2005).
36. M. S. Bilgili, *J. Hazard. Mater.*, **137**, 157 (2006).